IIETA International Information and Engineering Technology Association
Advancing the World of Information and Engineering

Traitement du Signal
Vol. 41, No. 6, December, 2024, pp. 2809-2821
Journal homepage: http://iieta.org/journals/ts

DoubleSENeXt: Investigations on Enchondroma Detection

Emine Yildirim Uslu[1*], Mustafa Yildirim[2], Rena Hajiyeva[3], Sengul Dogan[4], Turker Tuncer[4]

[1] Physical Medicine and Rehabilitation, Elazig Fethi Sekin City Hospital, Elazig 23100, Turkey
[2] Department of Radiology, Firat University Hospital, Elazig 23119, Turkey
[3] Department of Information Technologies, Western Caspian University, Baku 1001, Azerbaijan
[4] Department of Digital Forensics Engineering, College of Technology, Firat University, Elazig 23119, Turkey

Corresponding Author Email: sdogan@firat.edu.tr

https://doi.org/10.18280/ts.410604

Received: 1 August 2024
Revised: 31 October 2024
Accepted: 8 November 2024
Available online: 31 December 2024

Keywords:
CWINCA, DoubleSENeXt, enchondroma, exemplar deep feature engineering, tkNN

ABSTRACT

There are various deep learning models used to solve computer vision problems, with convolutional neural networks (CNNs) and transformers being commonly employed. However, these models have typically proposed by technological giants, and most researchers have relied on them. In this research, we aim to propose a new generation CNN model, termed Double Squeeze-and-Excitation Network (DoubleSENeXt), to address the stagnation in the development of new models. In this study, two new image classification models have been introduced: (i) DoubleSENeXt and (ii) an Exemplar Deep Feature Engineering (EDFE) model. The proposed DoubleSENeXt consists of four main stages: (1) stem, (2) main, (3) downsampling, and (4) output stages. Additionally, we have presented a lightweight version of the proposed DoubleSENeXt. The EDFE model comprises three main phases: (i) feature extraction with the pretrained DoubleSENeXt, (ii) feature selection using Cumulative Weighted Iterative Neighborhood Component Analysis (CWINCA), and (iii) classification with the tkNN algorithm-based k-nearest neighbors. Both new models have been applied to a newly collected enchondroma image dataset for classification. Both models achieved over 92% test classification accuracy on this dataset, with the proposed DoubleSENeXt reaching 92.15% test classification accuracy, and the EDFE model further improving this accuracy to 97.67%.

1. INTRODUCTION

Bone tumors are generally classified into two categories: enchondromas and chondrosarcomas. Enchondromas are benign, non-cancerous tumors, whereas chondrosarcomas are malignant, cancerous tumors [1, 2]. Determining whether a tumor is an enchondroma or a chondrosarcoma is critically important, as the treatment approach for enchondroma tumors differs significantly, while the treatment for chondrosarcoma tumors falls under cancer therapy. Thus, distinguishing between these types of bone tumors is crucial from a clinical perspective [3]. Bone tumor types are identified using MRI (magnetic resonance imaging), and the accuracy of this identification depends on the radiologist's experience and expertise. Additionally, there is no autonomous method currently used in hospitals or medical centers for identifying bone tumor types [4]. In MRI-based manual tumor detection, common challenges include the tumor being in an early stage, unclear imaging, and limited experience of the radiologist. To address these issues more efficiently, there is a need for autonomous assistants. The most suitable methods for developing such assistants are computer vision techniques [5].

In this research, the main focus is on detecting enchondromas. Therefore, some preliminary information about enchondromas is provided as follows: Enchondromas are among the most common benign bone tumors found in the medullary cavity of long bones, such as the tibia and femur [6]. These tumors are usually asymptomatic and non-aggressive. They require little to no treatment unless significant growth occurs, which can lead to bone weakening or pathological fractures [7, 8]. Although, chondrosarcomas require aggressive treatment due to their potential to metastasize, highlighting the importance of accurate early diagnosis [9].

To detect the bone tumor automatically, doctors and researchers have recently focused machine learning (ML)-based approaches [10-12]. ML-based computer aided models can detect the unseen patterns and to improve the detection accuracy [13]. ML-based model can extract the hidden patterns of the tumors [14, 15]. In this point, the ML models are valuable for automatic disorder detection [16]. Therefore, a deep learning (DL) model has been presented to detect enchondroma in this research.

1.1 Literature review

Many machine learning techniques have been developed in the literature to detect different diseases [17, 18]. However, there are limited studies in the literature on machine learning-based enchondroma detection. Current studies available in the literature are presented below.

Erdem et al. [19] proposed using radiomics and ML to differentiate chondrosarcoma from enchondroma by analyzing MRI data from 88 patients. The study extracted 1888 radiomic features per patient from T1 and PD (proton density) MRI sequences and employed various ML models, with the neural network showing the best performance. Their model achieved an area under the curve (AUC), accuracy, and F1 score of 97.90%, 98.40%; 92.00%, 93.20%; and 88.90, 90.30%, respectively. Cilengir et al. [20] assessed the diagnostic performance of MRI-based texture analysis for differentiating enchondromas and chondrosarcomas by segmenting tumor volumes from FS-PD and T1-weighted images and extracting 861 radiomic features. They found that the k-neighbors classifier performed best for FS-PD images. They attained an AUC of 1.00, accuracy of 80.00%, recall of 80.00%, precision of 100%, and F1 score of 89.00%. Anttila et al. [21] proposed a study to detect enchondromas from hand radiographs using a deep learning (DL) segmentation tool. Their study involved training a DL model with 414 enchondroma radiographs and testing it on a separate set of 131 radiographs, where 47% contained enchondromas. Their model obtained an AUC of 0.95 and an F1 score of 69.5%. Gitto et al. [22] proposed using MRI radiomics and ML to classify low-to-high grade cartilaginous bone tumors. They analyzed MRI data from 58 patients and used a Random Forest wrapper with the AdaboostM1 classifier and achieved an accuracy of 85.7% in the training set and 75.00% in the test set. Yoon et al. [23] suggested using SPECT/CT radiomics to tell enchondromas from grade I chondrosarcomas in long bones. They looked back at SPECT/CT data from 49 patients and analyzed 42 radiomics parameters. Using LASSO regression, they found that zone-length non-uniformity and coarseness were key features. These features showed 85.0% sensitivity and 58.3% specificity in the training set, and 83.3% sensitivity and 90.9% specificity in the test set. Their study showed that SPECT/CT radiomics could accurately distinguish between enchondromas and ACTs. Lisson et al. [24] suggested using 3D texture analysis from MRIs to tell apart low-grade chondrosarcoma from enchondroma. They evaluated MRIs from 22 patients, extracting texture features like kurtosis and entropy, and found significant differences between the two tumor types. The kurtosis in contrast-enhanced T1 images showed the highest discriminatory power with an AUC of 0.876, 82.00% sensitivity, 91.00% specificity, and 86.00% accuracy. Manganelli Conforti et al. [25] proposed a method to classify chondrogenic tumors using DL and wavelet transform of Raman spectra. They analyzed Raman spectra obtained from bone tissues of patients, using a technique called CLARA. Their method achieved high accuracy, recognizing and grading tumors with 97.00% accuracy. Gitto et al. [26] suggested using radiomics and ML on X-ray images to tell apart unusual cartilaginous tumors from high-grade chondrosarcomas in long bones. They looked back at X-rays from 150 patients at two centers. Their method separated the tumor types with 80% accuracy in both test groups, matching the accuracy of radiologists. von Schacky et al. [27] suggested using ML on X-ray data to tell apart benign from malignant bone tumors. They studied X-rays from 880 patients, with 213 having malignant and 667 benign tumors. Their approach achieved 80% accuracy, with an AUC of 0.79 for the internal test set and 0.90 for the external set.

1.2 Literature gaps and motivations of recommended model

In this section, we have first detected literature gaps, and based on these gaps, the motivation for this research has been provided.

Based on the reviewed literature, the identified literature gaps are:

- Most researchers have used well-known DL models such as ResNet [28], vision transformers (ViT) [29], DenseNet [30], etc. This has led to stagnation in the generation of new DL models [31-33], which are generally proposed by technology giants such as Meta, OpenAI, Google Brain, etc.
- There are various feature engineering models in the literature [34, 35]. However, these models have limited innovations due to the popularity of DL [36].
- There are a large number of automatic biomedical models based on ML [37, 38], but there are limited bone-based or orthopedic research studies based on ML [39-41].

Based on these gaps in the literature, our main motivations are as follows:

Firstly, we have proposed a next-generation CNN [42] model named DoubleSENeXt. In this model, two SE blocks are incorporated into the main stage to extract more meaningful features. Additionally, the presented CNN is a lightweight model, addressing the fact that most recent deep learning models tend to be large and computationally intensive. From this perspective, we have contributed to the development of lightweight CNN methodologies.

By introducing DoubleSENeXt, this research has made a contribution to the deep learning (DL) field. Additionally, we aimed to contribute to feature engineering. Therefore, we proposed a new Exemplar Deep Feature Engineering (EDFE) model. In this EDFE model, we drew inspiration from patch-based models such as Vision Transformer (ViT) and MLP Mixer [43]. Furthermore, three innovative machine learning (ML) methods were employed in the EDFE: Cumulative Weighted Iterative Neighborhood Component Analysis (CWINCA) for feature selection and t-algorithm-based k-nearest neighbors (tkNN) for classification. By proposing this EDFE, we successfully increased the test classification performance of the DoubleSENeXt model.

Finally, our motivation includes bridging the gap between bone imaging and machine learning models. Therefore, we collected a new enchondroma image dataset and used it as a testbed. Both proposed models were applied to this dataset, and the ability of the ML models to detect enchondroma was thoroughly investigated.

1.3 Contributions

- In this work, a new CNN model named DoubleSENeXt has been proposed. By introducing DoubleSENeXt, we have contributed to the CNN research area and presented a new lightweight model. Furthermore, this CNN model is scalable, and by adjusting parameters and repetitions, larger CNN models can be developed.
- To contribute to feature engineering, a next-generation EDFE model has been proposed. In this EDFE, we have utilized next-generation methods, including (i) CWINCA and (ii) tkNN.

- Both proposed models have been applied to the newly collected enchondroma MRI image dataset, achieving over 92% test classification accuracy (the proposed DoubleSENeXt attained 92.15%, while the recommended EDFE reached 97.67%).

2. DATASET

A new enchondroma MRI image dataset was collected from a single medical center. This dataset was gathered retrospectively, and the diagnoses were validated by both a radiologist and a physician. The dataset consists of two classes: (i) enchondroma and (ii) control. In this research, we proposed a new deep learning (DL) model. Therefore, the dataset was divided into two folders: (i) train and (ii) test. The distributions of the collected enchondroma image dataset are shown in Table 1.

Moreover, the example images have been demonstrated in Figure 1.

These sample images (see Figure 1) showcase the types of images included in the dataset, providing a visual context for the classification tasks undertaken in this research.

Table 1. The distribution of the collected MR image dataset

No	Class	Train	Test	Total
1	Enchondroma	549	139	688
2	Control	613	205	818
	Total	1162	344	1506

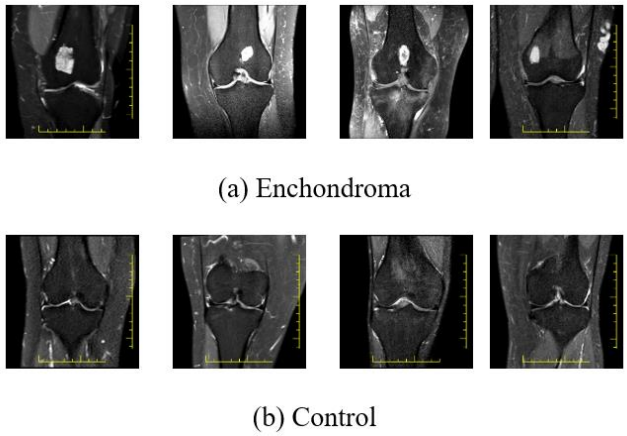

(a) Enchondroma

(b) Control

Figure 1. Sample images of the collected dataset

3. THE PROPOSED DOUBLESENEXT

The central focus of this research is the proposed DoubleSENeXt model. This work aimed to investigate the impact of double squeeze-and-excitation (SE) blocks on computer vision tasks, and we have developed a scalable version of this CNN model. A base version of the CNN was used in this research to demonstrate the classification capabilities of the proposed model. The graphical outline of the DoubleSENeXt model is shown in Figure 2.

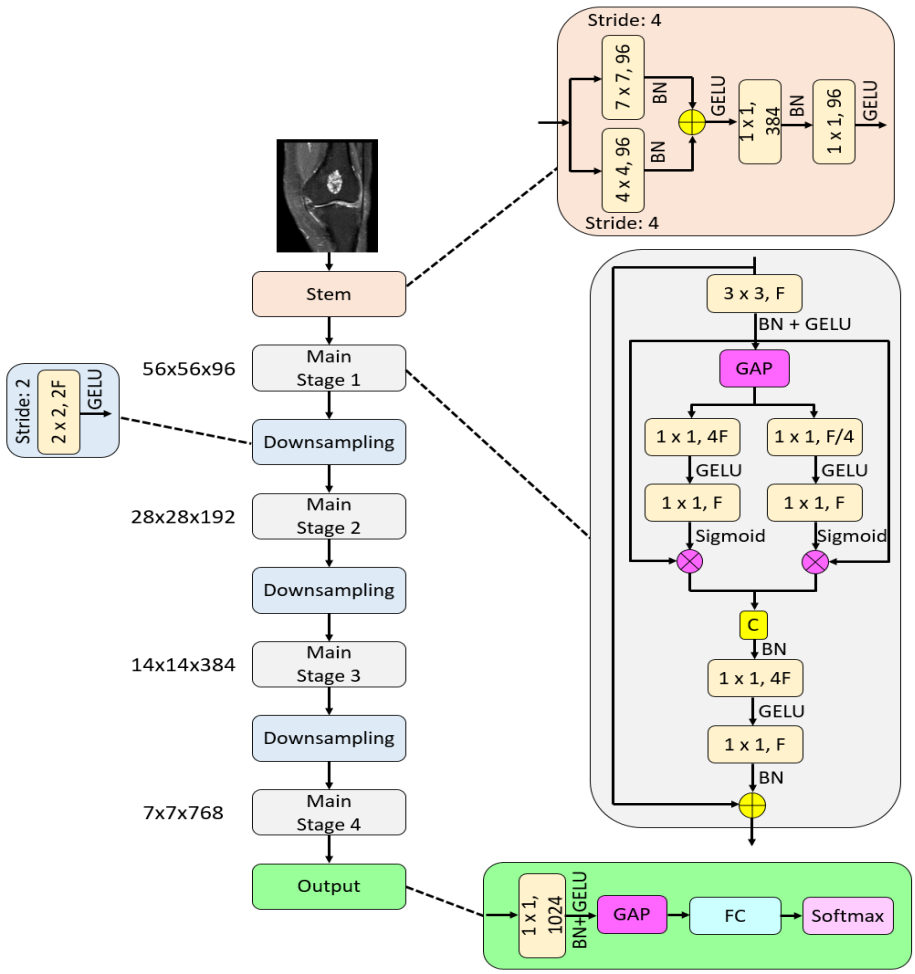

Figure 2. The graphical outline of the proposed DoubleSENeXt. Herein, F: number of filters, C: depth concatenation function, BN: batch normalization, GELU: Gaussian Error Linear Unit, GAP: global average pooling, FC: fully connected

The stages of this model are explained below.

Stem: The first stage of the proposed DoubleSENeXt is the stem block. We used two convolution operators: 4×4 and 7×7 convolutions. The 4×4 convolution defines the patchify block, while the 7×7 convolution is used as in ResNet50. By using both, we aimed to extract meaningful features. To integrate the features from these convolutions, an addition block was employed. The mathematical definition of the stem block in the proposed DoubleSENeXt is provided below:

$$S_1 = GELU(BN(C^{7\times7}_{96,Stride=4}(Im)) + BN(C^{4\times4}_{96,Stride=4}(Im))) \quad (1)$$

$$S_2 = BN\left(C^{1\times1}_{384}(S_1)\right) \quad (1a)$$

$$S_{out} = GELU\left(C^{1\times1}_{96}(S_2)\right) \quad (1b)$$

Herein, S: output of the stride block, Im: image, $C(.)$: convolution, $BN(.)$: batch normalization and $GELU(.)$: Gaussian Error Linear Unit. In this stage, a tensor with a size of 56×56×96 has been created from an image with a size of 224×224×3.

Main: The essential feature extraction block of the proposed DoubleSENeXt is the main block. In this block, double SE blocks have been added to a ConvNeXt-like block. We used concatenation, multiplication, and addition operators in this block. The mathematical definitions of this block are as follows:

$$Out_i = GELU\left(BN\left(C^{3\times3}_F(Out_{i-1})\right)\right) \quad (2)$$

$$Flat = GAP(Out_i) \quad (2a)$$

$$SE_1 = Sigmoid\left(C^{1\times1}_F\left(GELU\left(C^{1\times1}_{4F}(Flat)\right)\right)\right) \times Out_i \quad (2b)$$

$$SE_2 = Sigmoid\left(C^{1\times1}_F\left(GELU\left(C^{1\times1}_{F/4}(Flat)\right)\right)\right) \times Out_i \quad (2c)$$

$$Out_{i+1} = BN\left(Concat(SE_1, SE_2)\right) \quad (2d)$$

$$Out_{i+2} = GELU\left(C^{1\times1}_{4F}(Out_{i+1})\right) \quad (2e)$$

$$Out_{i+3} = BN\left(C^{1\times1}_F(Out_{i+2})\right) + Out_{i-1} \quad (2f)$$

where, Out: output of the operations, $GAP(.)$: global average pooling function, $Flat$: flatten output, SE: output of the SE blocks. Herein, two SE blocks with different parameters have been used, and the outputs of these SE blocks have been concatenated to utilize their combined outputs. Specifically, we have enhanced the ConvNeXt block by using double SE blocks and reduced the number of parameters by using 3×3 sized convolutions instead of 7×7 sized convolutions.

Downsampling: In this stage, we used a patchify operation to decrease the size of the tensor and increase its depth. Therefore, a 2×2 convolution with a stride of 2 was applied.

$$Dout = GELU(C^{2\times2}_{2F}(Out_k)) \quad (3)$$

Herein, $Dout$: output of the downsampling stage.

Table 2. Transition of the proposed DoubleSENeXt

Layer	Input	Operation	Output
Stem	224×224×3	(4×4, 96, BN, stride: 4)+(7×7, 96, BN, stride: 4)+GELU 1×1, 384, BN 1×1, 96, GELU	56×56×96
Main 1	56×56×96	$\begin{bmatrix} 3\times3,96 \\ 1\times1,384, 1\times1,24 \\ 1\times1,96, 1\times1,96 \\ 1\times1,384 \\ 1\times1,96 \end{bmatrix}$	56×56×96
Downsampling 1	56×56×96	2×2, 192, stride: 2, GELU	28×28×192
Main 2	28×28×192	$\begin{bmatrix} 3\times3,192 \\ 1\times1,768, 1\times1,48 \\ 1\times1,192, 1\times1,192 \\ 1\times1,768 \\ 1\times1,192 \end{bmatrix}$	28×28×192
Downsampling 2	28×28×192	2×2, 384, stride: 2, GELU	14×14×384
Main 3	14×14×384	$\begin{bmatrix} 3\times3,384 \\ 1\times1,1536, 1\times1,96 \\ 1\times1,384, 1\times1,384 \\ 1\times1,1536 \\ 1\times1,384 \end{bmatrix}$	14×14×384
Downsampling 3	14×14×384	2×2, 768, stride: 2, GELU	7×7×768
Main 4	7×7×768	$\begin{bmatrix} 3\times3,768 \\ 1\times1,3072, 1\times1,192 \\ 1\times1,768, 1\times1,768 \\ 1\times1,3072 \\ 1\times1,768 \end{bmatrix}$	7×7×768
Output size	7×7×768	1×1, 1024, BN, GELU, GAP, FC, Softmax	Number of classes
Total learnable parameters			8.9 Million

Output: The classification stage of the proposed model is the output stage. In this stage, we used a 1×1 convolution with a filter of 1024 to increase the number of features. Following that, Global Average Pooling (GAP), fully connected, and SoftMax blocks were applied to obtain the classification result. The mathematical explanations of this stage are as follows:

$$fm = GELU(BN(C_{1024}^{1\times1}(Out_h))) \quad (4)$$

$$Out = Softmax\left(FC\left(GAP(fm)\right)\right) \quad (4a)$$

where, fm: feature matrix, $FC(.)$: fully connected layer and Out: the output of the presented network.

Per the explained stages, the transition table of the proposed DoubleSENeXt is tabulated in Table 2.

4. THE PROPOSED EXEMPLAR DEEP FEATURE ENGINEERING MODEL

To investigate the transfer learning ability of the proposed DoubleSENeXt, a new EDFE model has been proposed. This model consists of three phases:

- Exemplar deep feature extraction deploying the pretrained DoubleSENeXt.
- Feature selection by deploying CWINCA [44, 45].
- Classification by deploying tkNN with 10-fold cross-validation [44].

In the first phase, the pretrained DoubleSENeXt was utilized as a feature extractor, and the final GAP layer of this model was used as the feature extraction layer. To extract features in detail, we employed a semi-overlapping block approach, with each block sized at 56×56×3 and a stride of 28. This generated 49 semi-overlapping patches. Additionally, the features of the raw image were extracted as the 50th feature vector. These feature vectors were merged to create the final feature vector with a length of 51,200(=50×1024).

For feature selection, the CWINCA feature selector was applied to the generated 51,200 features. The main advantage of CWINCA is its ability to automatically detect the range of iterations by using the cumulative weights of the features.

In the final phase, the selected features were used as input for the tkNN classifier, an iterative ensemble classifier.

To further explain the proposed EDFE model, a graphical outline is shown in Figure 3.

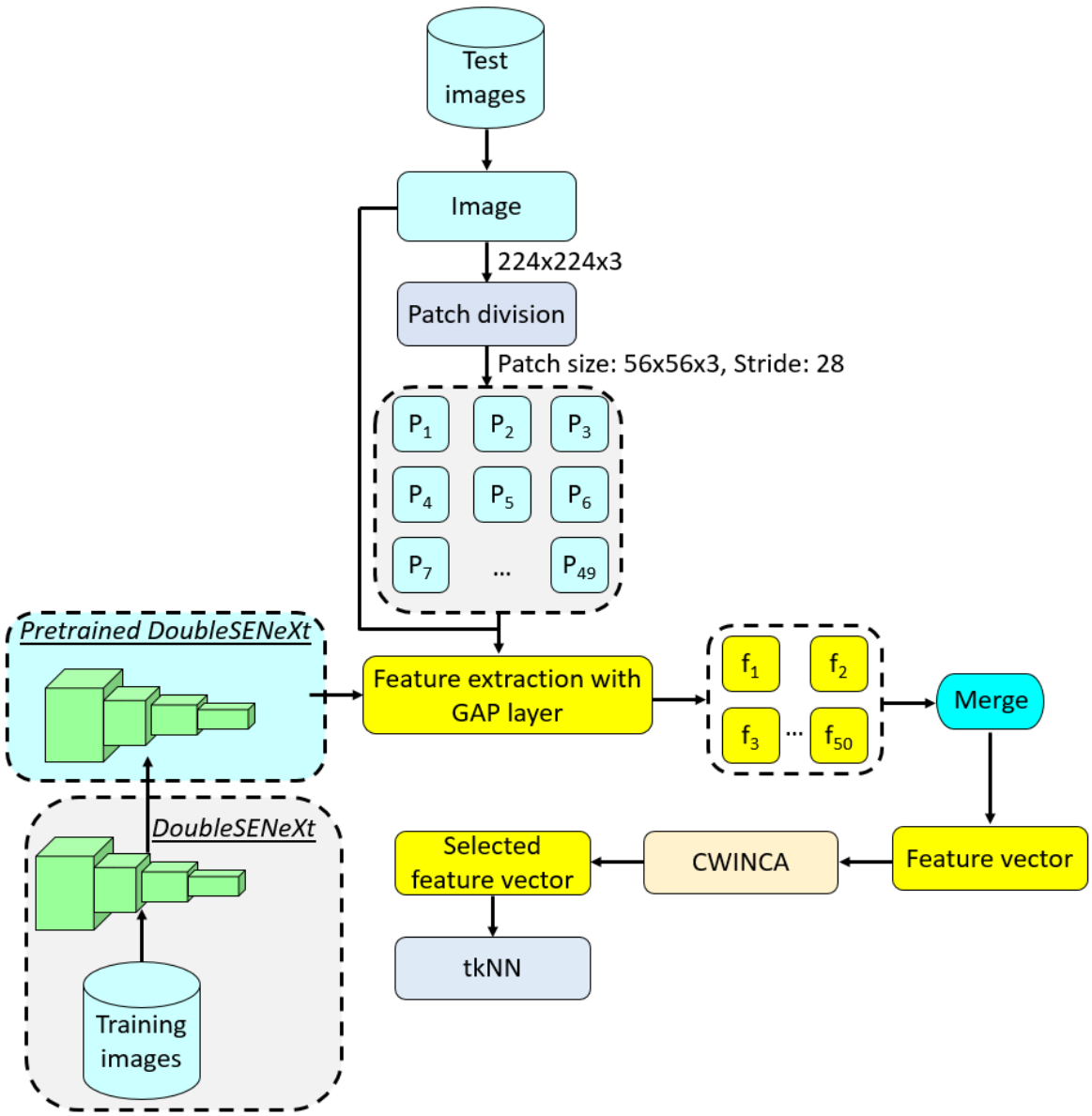

Figure 3. Block diagram of the proposed EDFE. Herein, P: Patch, f: feature vectors with a length of 1024

To better explain the proposed EDFE model, the steps of this model are as follows:

Feature extraction: The first phase of this EDFE model is feature extraction, during which 51,200 features were extracted for each image. These features were derived from semi-overlapping blocks. Consequently, this deep feature engineering model is considered an exemplar deep feature engineering model. The steps of this phase are as follows:

Step 1: Train the training phase of the collected dataset deploying the recommended DoubleSENeXt.

Step 2: Read each test image.

Step 3: Create the semi-overlapped patches from the test image.

$$patch_{q,t} = Im(i{:}\, i + 56q - 1, j{:}\, j + 56t - 1), \tag{5}$$

$$i \in \{1{,}29, \dots 224 - 28\}, j \in \{1{,}29, \dots 224 - 28\}, \quad q \in \{1{,}2, \dots, 7\}, t \in \{1{,}2, \dots, 7\} \tag{5a}$$

$$P_w = patch_{q,t}, w \in \{1{,}2, \dots, 49\} \tag{5b}$$

where, $patch$: created patches, P: patch array and Im: test image.

Step 4: Extract features deploying the pretrained DoubleSENeXt.

$$f_1 = DoubleSENeXt(Im, GAP) \tag{6}$$

$$f_{w+1} = DoubleSENeXt(P_w, GAP) \tag{6a}$$

where, f: individual feature vector with a length of 1024.

Step 5: Merge the generated individual feature vectors.

$$F = concat(f_1, f_2, \dots, f_{50}) \tag{7}$$

Here F: in the final feature vectors with a length of 51,200.

Step 6: Repeat Steps 1-5 for each image until all images have been processed and a complete feature matrix is obtained.

Feature selection: The main feature selection function used is CWINCA [44], a developed version of the INCA [46] feature selector. By utilizing cumulative weights, the range of the loop is determined, and within this range, iterative feature selection is performed. This feature selector is greedy-based, as it selects the feature vector with the minimum misclassification ratio.

CWINCA was selected as the feature selection method for its ability to iteratively select the most informative features from a large feature set, which is crucial for high-dimensional data such as MRI images. Unlike traditional feature selection techniques, which focus on global variance or separability, CWINCA leverages the cumulative weights of the features to iteratively refine the selection. This method is an enhancement over standard NCA as it automatically determines the range of iterations, making it more adaptive to the data. Its cumulative weighting approach ensures that only the most relevant features are retained, improving the overall classification performance while reducing computational complexity.

The steps of the CWINCA selector used are as follows:

Step 7: Create the qualified indexes of the and generated weights of the features by utilizing NCA [47] feature selector. NCA feature selector is a distance-based feature selector. Thus, minimum and maximum normalization has been utilized to the feature matrix.

$$X^N(:,i) = \frac{X(:,i) - X(:,i)_{min}}{X(:,i)_{max} - X(:,i)_{min}}, i \in \{1{,}2, \dots, 51200\} \tag{8}$$

$$[ind, wg] = NCA(X^N, y) \tag{8a}$$

Herein, X^N: the normalized feature matrix, $X(:,i)_{max}$: maximum value of the used feature column, $X(:,i)_{min}$: minimum value of the used feature column, ind: the sorted indices, wg: weight of the features, $NCA(.)$: NCA feature selection function and y: actual outputs.

Step 8: Compute the start and stop values of the loop by utilizing cumulative weights.

$$id = argsort(-wg) \tag{9}$$

$$wg_{cum} = \frac{\sum_{i=1}^{k} wg_{id(i)}}{\sum_{j=1}^{n} wg_j}, k \in \{1{,}2, \dots, n\} \tag{9a}$$

$$start = \begin{cases} \min\{i | wg_{cum} \geq 0.95 \\ 10 \end{cases} \tag{9b}$$

$$stop = \begin{cases} \min\{i | wg_{cum} \geq 0.999 \\ Size(X, 2) \end{cases} \tag{9c}$$

where, id: the indices of the features sorted by their weights in descending order, wg_{cum}: cumulative weights, $start$: start value of the loop and we have used 0.95 as threshold value, $stop$: stop value of the loop and 0.999 has been utilized as the threshold value.

Step 9: Select features iteratively using start and stop values.

$$fs^{r-start+1}(d,h) = X^N\big(d, ind(h)\big), \tag{10}$$

$$r \in \{start, start + 1, \dots, stop\}, d \in \{1{,}2, \dots, NI\}, \quad h \in \{1{,}2, \dots, r\} \tag{10a}$$

Herein, fs: selected feature vector and NI: number of images.

Step 10: Compute the misclassification rate of each selected feature vector by utilizing kNN classifier and select a feature vector with the minimum misclassification ratio.

$$mcr(r - start + 1) = kNN(fs^{r-start+1}, y) \tag{11}$$

$$ix = \min(mcr) \tag{11a}$$

$$fsel = fs^{ix} \tag{11b}$$

where, mcr: misclassification ratio, $kNN(.)$: kNN classifier, ix: index of the minimum misclassification ratio and $fsel$: final selected feature vector.

Classification: In the classification phase, an iterative ensemble classifier named tkNN has been used, which employs the t algorithm. In the t algorithm, by changing the parameters of kNN [48], multiple classification outputs are generated, referred to as parameter-based outputs. Then, the Iterative Majority Voting (IMV) [49] algorithm is applied to these parameter-based outputs, generating voted outputs. In the final phase, the output with the highest classification accuracy is selected as the final result.

The tkNN classifier was chosen for its iterative nature and ability to generate multiple classification outputs by varying

key parameters such as distance metrics, weighting schemes, and the number of neighbors (k). Traditional kNN methods can be limited by sensitivity to parameter selection, which can affect classification accuracy. tkNN addresses this limitation by generating an ensemble of outputs, which are then refined using Iterative Majority Voting (IMV). This approach enhances robustness and accuracy, particularly in cases where class distributions may vary, or noise is present. Compared to other classifiers, tkNN provides a more flexible and adaptive framework for classification in biomedical datasets, where small differences in features can have a significant impact on the results.

The steps of the tkNN classifier are as follows:

Step 11: Generate parameters-based outputs.

$$\mathcal{D} \in \{"cityblock", "euclidean", "minkowski", "spearman", "correlation", "cosine"\} \quad (12)$$

$$\mathcal{W} \in \{"SquaredInverse", "Inverse", "Equal"\} \quad (12a)$$

$$\mathcal{K} \in \{1,2,\dots,5\} \quad (12b)$$

$$Pout_q = kNN(fsel, \mathcal{D}_i, \mathcal{W}_j, \mathcal{K}_t), i \in \{1,2,\dots,6\} \quad (12c)$$

$$j \in \{1,2,3\}, t \in \{1,2,\dots,5\}, q \in \{1,2,\dots,90\} \quad (12d)$$

Herein $Pout$: parameters-based outcomes and 90 outcomes have been created by utilizing the given parameters.

Step 12: Apply IMV to the generated parameters-based outputs and generated voted outputs and select the best output per the classification accuracies.

$$acc_q = \beta(Pout_q, y) \quad (13)$$

$$x = argsort(-acc) \quad (13a)$$

$$VOut_{h-2} = \varpi(POut_{x(1)}, POut_{x(2)}, \dots, POut_{x(h)}), \; h \in \{3,4,\dots,90\} \quad (13b)$$

$$acc_{90+c} = \beta(Vout_c, y), c \in \{1,2,\dots,88\} \quad (13c)$$

$$mx = argmax(acc) \quad (13d)$$

$$FOut = \begin{cases} POut_{mx}, mx \le 90 \\ VOut_{mx-90}, mx > 90 \end{cases} \quad (13e)$$

where, acc: classification accuracies, $\beta(.)$: classification accuracy calculation function, $VOut$: voted outcomes. In this research, the range of iteration of the IMV has been selected from 3 to 90. Therefore, 88(=90-3+1) voted outcomes have been created. mx: index of the maximum accuracy and $FOut$: final outcome.

The 12 steps given above define the proposed EDFE model.

In the presented EDFE model, CWINCA and tkNN were selected for their complementary strengths in feature selection and classification. CWINCA effectively reduces the feature space while retaining discriminative power, and tkNN ensures robust and accurate classification by using an ensemble-based approach. Moreover, both methods are self-organized since they generate more than one output and select the best outcome.

5. EXPERIMENTAL RESULTS

Two novel methods have been proposed in this research, with the primary model being the DoubleSENeXt CNN. First, we designed the DoubleSENeXt using MATLAB Deep Network Designer. We utilized 108 layers and 124 connections to develop DoubleSENeXt. Afterward, the proposed CNN was trained on the training set of the collected enchondroma dataset, and the trained DoubleSENeXt was stored as a mat file, which was then used as the feature extraction function in the proposed EDFE model. To train the DoubleSENeXt, we used the following parameters:

Solver: SGDM (stochastic gradient descent momentum)
Initial learning rate: 0.01
Mini-batch size: 128
Maximum epoch: 100
L2 Regularization: 0.001
Gradient threshold method: L2 Norm
Learning rate drop factor: 0.1
Testing and validation split ratio: 80:20

Using the parameters listed above, the obtained training and validation curves are demonstrated in Figure 4.

As shown in Figure 4, the proposed DoubleSENeXt achieved 100% training accuracy, 0 training loss, 91.38% final validation accuracy, and 0.2811 final validation loss. Using this pretrained DoubleSENeXt, the test classification accuracies of both the recommended DoubleSENeXt and the recommended EDFE were evaluated. The confusion matrices of these models are presented in Figure 5.

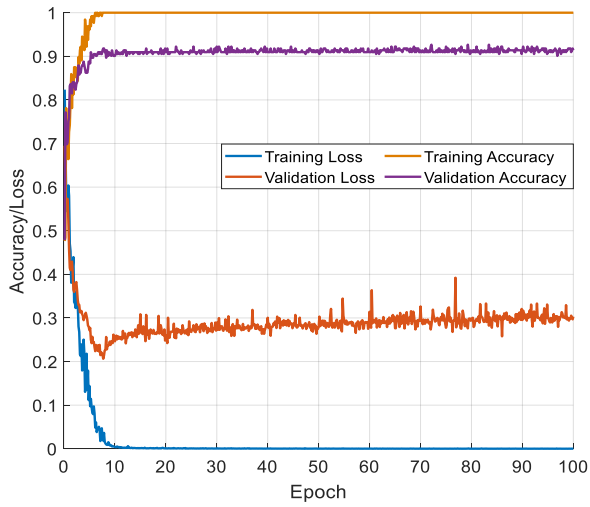

Figure 4. Training and validation curve of the proposed DoubleSENeXt model

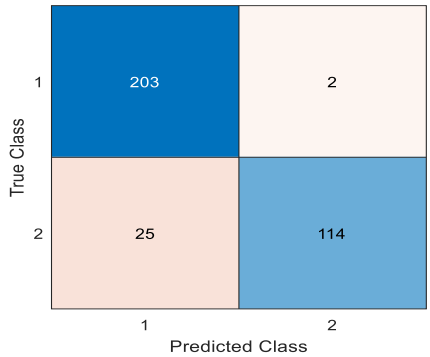

(a)

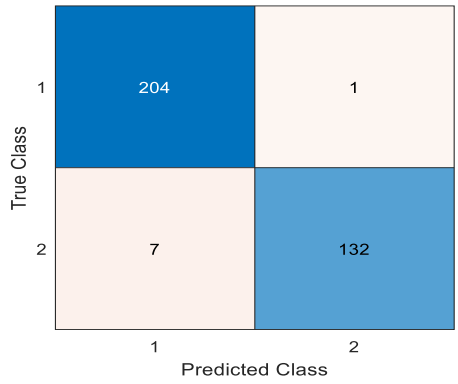

(b)

Figure 5. Test confusion matrices of the proposed models (a) DoubleSENeXt, (b) DoubleSENeXt-based EDFE. Herein, 1: Control, 2: Enchondroma

As shown in Figure 5, the proposed EDFE has improved the test classification performance of the DoubleSENeXt. Moreover, to comprehensively evaluate these test results, sensitivity, specificity, geometric mean, and accuracy values were computed. These values are listed in Table 3.

Table 3 shows that the proposed EDFE model increased the test classification accuracy of the DoubleSENeXt by 5.52 percentage points. Moreover, this EDFE model improved the geometric mean by 7.08 percentage points. These results clearly demonstrate the classification capabilities of the CWINCA and tkNN models. Additionally, the recommended EDFE model achieved this high classification performance using only 141 features out of the generated 51,200 features.

To illustrate the explainable attributes of the proposed DoubleSENeXt, sample images and Gradient-weighted Class Activation Mapping (Grad-CAM) were used. By utilizing these methods, heat maps of the images were generated to highlight the regions of interest identified by the proposed model. These results are demonstrated in Figure 6.

Figure 6 clearly demonstrates that the proposed DoubleSENeXt can focus on the region of interest. By using a patch-based model, we have increased the classification ability of the proposed DoubleSENeXt.

Table 3. Transition of the proposed DoubleSENeXt

DoubleSENeXt		
Performance metric	Class	Result
Sensitivity	Enchondroma	82.01
	Control	99.05
	Overall	90.53
Specificity	Enchondroma	99.05
	Control	82.01
	Overall	90.53
Geometric mean	Overall	90.13
Accuracy	Overall	92.15
DoubleSENeXt-based EDFE		
Sensitivity	Enchondroma	94.96
	Control	99.51
	Overall	97.24
Specificity	Enchondroma	99.51
	Control	94.96
	Overall	97.24
Geometric mean	Overall	97.21
Accuracy	Overall	97.67

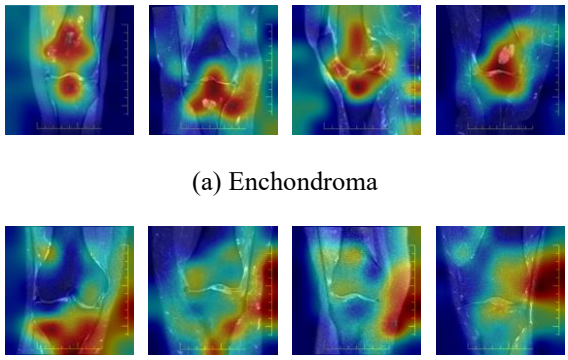

(a) Enchondroma

(b) Control

Figure 6. Heat maps generated by Grad-CAM activation

6. DISCUSSION

We have introduced two novel models along with a newly collected enchondroma MR image dataset. Both proposed models achieved over 92% test classification accuracy on the collected dataset. Additionally, explainable results have been demonstrated using Grad-CAM, providing insights into the regions of interest that contributed to the classification decisions.

The recommended DoubleSENeXt model is a lightweight model as it has fewer than 10 million parameters. Moreover, the presented EDFE model aims to increase test classification accuracy. The presented EDFE uses pretrained DoubleSENeXt, CWINCA, and tkNN. Therefore, its time complexity is $O(ND + C + t)$, where D, C, and t represent the time complexity coefficients of the pretrained DoubleSENeXt-based deep feature extractor, CWINCA, and tkNN, respectively and N is number of patches.

First, we conducted an ablation study on the proposed DoubleSENeXt. In this CNN model, two SE blocks were incorporated: the first SE block is termed SE 0.25, and the second is SE 4. To assess their individual contributions, we tested the model with each SE block configuration, and the corresponding validation accuracies are as follows:

CNN 1: SE 0.25-based CNN.

CNN 2: SE 4-based CNN.

CNN 3: The proposed DoubleSENeXt (which combines both SE blocks).

The computed validation accuracies for these configurations are shown in Figure 7.

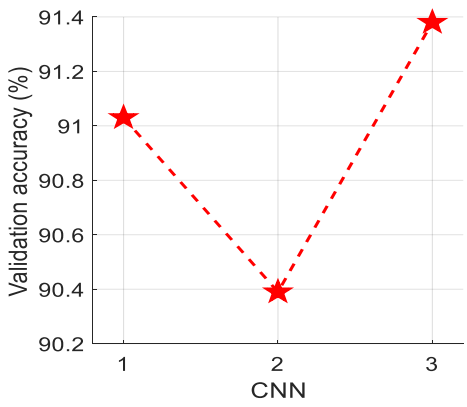

Figure 7. Validation accuracies of the defined CNNs

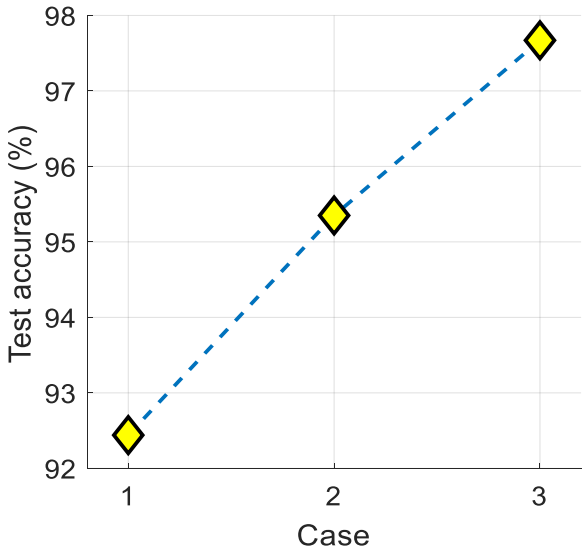

Figure 8. Classification accuracies of the defined cases

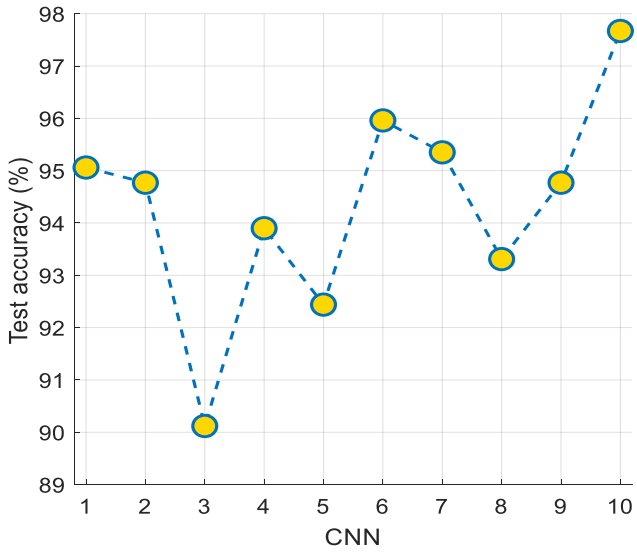

Figure 9. Test classification results of the CNNs on the used dataset

Table 4. Comparative results

Study	Methods	Classifier	Split Ratio	Data	Result(s) %
Jabber et al. [50]	Fuzzy C-Means, Back Propagation Neural Network	SVM	70:30	Cancer: 100 Normal: 100	Acc: 92.00 Sen: 93.00 Spe: 91.00
Anand et al. [51]	Deep convolutional extreme ML	Ensemble classifier	10 fold CV	Necrotic Tumor: 263 Non- Tumor: 536 Viable- Tumor: 345	Acc: 97.27 Sen: 98.20 Spe: 99.57
Our method	DoubleSENeXt	tkNN	10 fold CV	Control: 205 Enchondroma: 139	Acc: 92.15 Sen: 90.53 Spe: 90.53 GM: 90.13
	DoubleSENeXt-based EDFE				Acc: 97.67 Sen: 97.24 Spe: 97.24 GM: 97.21

Figure 7 demonstrates that the SE 0.25 block performs better than the SE 4 block. Therefore, the SE 0.25 block has been widely adopted in the literature. However, our proposed DoubleSENeXt outperforms both configurations.

On the other hand, to illustrate the classification impact of the CWINCA and tkNN classifier, ablation cases for the proposed EDFE have been defined as follows:

Case 1: Feature extraction with pretrained DoubleSENeXt and classification with kNN.

Case 2: Feature extraction with pretrained DoubleSENeXt, feature selection using CWINCA, and classification with kNN.

Case 3: Our proposed EDFE model (which combines feature extraction, CWINCA, and tkNN).

The test accuracy of these models is shown in Figure 8.

Figure 8 demonstrates that the recommended model (our proposed EDFE) achieved the highest classification accuracy, clearly highlighting the effectiveness of the CWINCA and tkNN methods.

To showcase the position of the proposed model within the existing literature, the comparative results have been presented in Table 4. This table provides a comparison of the classification performances of various methods, emphasizing the advantages of the proposed EDFE model in terms of accuracy and efficiency.

According to Table 4, the proposed model attained satisfactory classification performance for enchondroma MR image classification.

Furthermore, the computed results of the EDFE model have been demonstrated using other commonly used CNNs. In this regard, we changed the feature extractor to obtain comparative results. The CNNs utilized as feature extractors in the recommended EDFE are: (1) MobileNetV2, (2) ResNet50, (3) DarkNet53, (4) AlexNet, (5) ShuffleNet, (6) DenseNet201, (7) InceptionV3, (8) InceptionResNetV2, (9) GoogLeNet, and (10) the presented DoubleSENeXt. The computed test classification accuracies on the presented self-organized EDFE model are shown in Figure 9.

Figure 9 clearly demonstrates that the best-performing CNN among the 10 used CNNs is the presented DoubleSENeXt, which achieved 97.67% classification accuracy with the recommended EDFE structure. The worst-performing CNN is DarkNet53, as the DarkNet53-based EDFE reached 90.12% test accuracy. The best of the others (excluding the recommended DoubleSENeXt) is DenseNet201, as this CNN-based EDFE attained 95.93% test classification accuracy on this dataset.

This results (see Figure 9) highlights the effectiveness of the dual SE blocks integrated into the ConvNeXt-like structure of DoubleSENeXt. The dual SE blocks likely contribute to a better feature extraction by emphasizing informative features and suppressing irrelevant ones.

The results presented in Figure 9 provide a roadmap for

future work in biomedical image classification. First, the strong performance of DoubleSENeXt suggests that future models for tasks like enchondroma detection should incorporate mechanisms for recalibrating feature importance, such as SE blocks or attention mechanisms. Second, the efficiency of lightweight models like DoubleSENeXt demonstrates that there is no need for excessively large architectures to achieve high performance, which is critical for deployment in environments with limited computational resources, such as hospitals or clinics.

6.1 Test of the additional dataset

In order to show the general classification ability of the recommended model, we have used an additional dataset and this dataset is the blood cell image dataset. This dataset contains 17,092 blood cell images with eight categories and the distribution of this dataset is: basophils (1218), eosinophils (3117), erythroblasts (1551), immature granulocytes (2895), lymphocytes (1214), monocytes (1420), neutrophils (3329), and platelets (2348). The training and test split ration is defined as 75:25. Moreover, the training process is shown in Figure 10.

According to Figure 10, the recommended DoubleSENeXt achieved a final validation accuracy of 95.35% and a final validation loss of 0.0983. Furthermore, the test classification accuracy of the recommended DoubleSENeXt was calculated to be 96.59%. The corresponding test confusion matrix for the presented DoubleSENeXt is displayed in Figure 11.

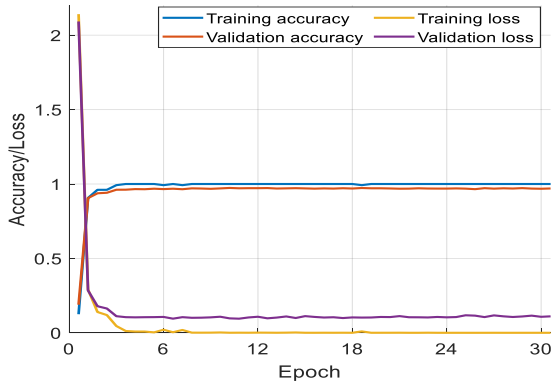

Figure 10. The training and validation curve of the recommended DoubleSENeXt

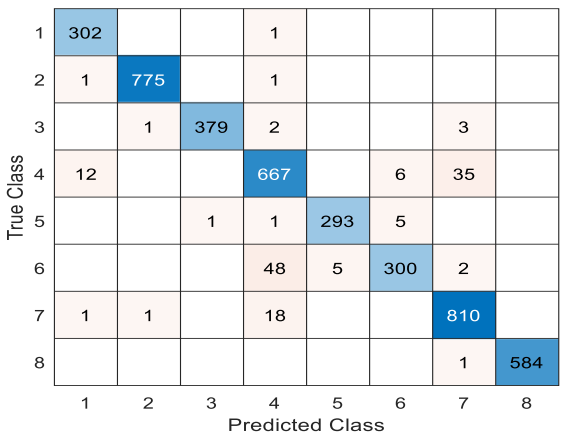

Figure 11. The test classification accuracy of the recommended DoubleSENeXt on the blood cell image dataset

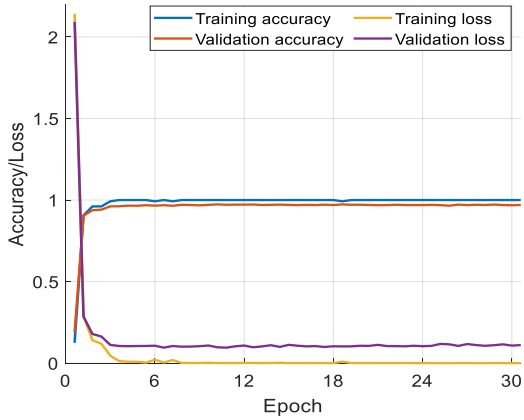

Figure 12. The comparative results. The cases are explained as follows. 1: VGG16+ SVM, 2: InceptionV3 + SVM, 3: VGG16 + Softmax, 4: InceptionV3 + Softmax, 5: The presented DoubleSENeXt

The computed test classification result was compared to the method of Acevedo et al. [52] and the computed results have been compared in Figure 12.

In Figure 12, cases 1-4 correspond to Acevedo et al.'s method, where their best-performing model, VGG16+Softmax (Case 3), achieved 96.2% accuracy. In comparison, our proposed DoubleSENeXt attained a higher classification accuracy of 96.59%. Despite being a lightweight model, the recommended DoubleSENeXt outperformed other non-lightweight CNNs in terms of classification accuracy.

6.2 Highlights

The important points of this research are also discussed below:

- In this research, a new lightweight CNN model has been proposed, termed DoubleSENeXt, which integrates double SE blocks into a modified ConvNeXt block.
- The proposed DoubleSENeXt is a scalable model, allowing larger CNN models to be developed by adjusting its parameters.
- ConvNeXt-inspired modifications were incorporated into the model to balance simplicity and performance.
- By using the recommended DoubleSENeXt, an EDFE model has been proposed. In our proposed EDFE model, we used two novel ML methods: (i) CWINCA and (ii) tkNN.
- The introduced EDFE model has linear time complexity due to its use of transfer learning.
- The self-organizing capabilities of CWINCA and tkNN enable the model to generate multiple outputs and automatically select the best one.
- Both presented models (DoubleSENeXt and EDFE) achieved high classification performance on the newly collected enchondroma dataset, with test accuracies exceeding 92%.
- The recommended EDFE model improved the test classification accuracy of DoubleSENeXt by 5.52 percentage points and the geometric mean by 7.08 percentage points, using only 141 selected features and the tkNN (iterative ensemble classifier).
- Ablation studies comparing the performance of different SE block configurations showed that the SE 0.25 block outperforms the SE 4 block, and

DoubleSENeXt surpasses both. Additionally, the combination of methods in the EDFE model proved to be the best for achieving high test classification accuracy.

- Grad-CAM was used to generate heat maps, highlighting the regions of interest (ROI) that the DoubleSENeXt model focused on during classification.
- The results clearly demonstrate that the proposed models can be applied in real-world environments to detect bone abnormalities.
- The recommended DoubleSENeXt outperformed nine commonly used CNNs on this dataset.
- The blood cell image dataset, used to test the generalizability of DoubleSENeXt, further demonstrated the model's versatility across different biomedical image classification tasks, achieving 96.59% accuracy in blood cell image classification.

7. CONCLUSIONS

The main motivation of this research is to introduce DoubleSENeXt, a new CNN, and to demonstrate its performance on a biomedical image dataset. To enhance the visibility of the proposed deep learning (DL) model, a new enchondroma MRI image dataset was collected, and the results from this dataset are presented in the article. An Exemplar Deep Feature Engineering (EDFE) model is also proposed to demonstrate the transfer learning capabilities of DoubleSENeXt. In this regard, this article contributes to both DL and feature engineering research areas.

Both models were applied to the collected enchondroma dataset, with DoubleSENeXt achieving a test accuracy of 92.15%, while the DoubleSENeXt-based EDFE model achieved an even higher accuracy of 97.67%. These results show that the lightweight DL model and the EDFE method based on it possess high classification capabilities. Furthermore, the explainable features of DoubleSENeXt were demonstrated through Grad-CAM, providing visual insight into the areas of focus within the model. The architecture's performance was further validated through ablation studies.

The primary reason for the 5.52% increase in accuracy using the EDFE model is attributed to the innovative CWINCA and tkNN methods. These findings, along with the results obtained, clearly highlight the effectiveness of the proposed methods. The study emphasizes that by further developing these models, intelligent enchondroma detection assistants could be created for real-world applications in hospitals. Future investigations will explore the classification capabilities of the proposed models on other biomedical images and public image datasets such as CIFAR and ImageNet.

ETHICAL APPROVAL

The Non-Invasive Ethics Committee, Firat University, approved this research on ethical grounds on August 8, 2024 (2024/ 08-08).

REFERENCES

[1] Zając, W., Dróżdż, J., Kisielewska, W., Karwowska, W., Dudzisz-Śledź, M., Zając, A.E., Borkowska, A., Szumera-Ciećkiewicz, A., Szostakowski, B., Szostakowski, B., Rutkowski, P., Czarnecka, A.M. (2023). Dedifferentiated chondrosarcoma from molecular pathology to current treatment and clinical trials. Cancers, 15(15): 3924.

[2] Fitzpatrick, J.D., Azzopardi, C., Ritchie, D.A., Davies, A.M., Vanel, D. (2023). Tumors and tumorlike lesions. In Imaging of the Foot and Ankle. Medical Radiology, Springer, Cham. https://doi.org/10.1007/174_2023_394

[3] Rai, V., Munazzam, S.W., Wazir, N.U., Javaid, I. (2024). Revolutionizing bone tumor management: Cutting-edge breakthroughs in limb-saving treatments. European Journal of Orthopaedic Surgery & Traumatology, 34(4): 1741-1748. https://doi.org/10.1007/s00590-024-03876-z

[4] Van Den Berghe, T., Delbare, F., Candries, E., Lejoly, M., Algoet, C., Chen, M., Laloo, F., Huysse, W.C.J., Creytens, D., Verstraete, K.L. (2024). A retrospective external validation study of the Birmingham Atypical Cartilage Tumour Imaging Protocol (BACTIP) for the management of solitary central cartilage tumours of the proximal humerus and around the knee. European Radiology, 1-19. https://doi.org/10.1007/s00330-024-10604-y

[5] Dau, G., McCool, I., Parker, L., Knollmann-Ritschel, B. (2023). Educational case: Cartilaginous tumors of bone. Academic Pathology, 10(2). https://doi.org/10.1016/j.acpath.2023.100070

[6] Goni, V.G., Bachhal, V., Kumar, D., Kataria, M. (2024). Bone tumors: An overview. Molecular Biomarkers for Cancer Diagnosis and Therapy, Springer, Singapore, 421-434. https://doi.org/10.1007/978-981-99-3746-2_20

[7] Lee, H., Wang, A., Cheng, R., Moran, J., Al-Dasuqi, K., Irshaid, L., Maloney, E., Porrino, J. (2023). Update of pediatric bone tumors-notochordal tumors, chondrogenic tumors, and vascular tumors of the bone. Skeletal Radiology, 52(6): 1101-1117. https://doi.org/10.1007/s00256-022-04235-x

[8] Abdelhalim, M., Linkwinstar, J., Rajakulasingam, R., Perera, J.R., Saifuddin, A., Pollock, R. (2023). Management of paediatric benign bone tumour. Paediatrics and Child Health. https://doi.org/10.1016/j.paed.2023.08.003

[9] Alexiev, B.A., Vormittag-Nocito, E.R., Peabody, T.D., Samet, J., Laskin, W.B. (2023). Clear cell chondrosarcoma: A review of clinicopathologic characteristics, differential diagnoses, and patient management. Human Pathology, 139: 126-134. https://doi.org/10.1016/j.humpath.2023.06.004

[10] Du, Y., McNestry, C., Wei, L., Antoniadi, A.M., McAuliffe, F.M., Mooney, C. (2023). Machine learning-based clinical decision support systems for pregnancy care: A systematic review. International Journal of Medical Informatics, 173: 105040. https://doi.org/10.1016/j.ijmedinf.2023.105040

[11] Subhan, S., Malik, J., ul Haq, A., Qadeer, M.S., Zaidi, S.M.J., Orooj, F., Zaman, H., Mehmoodi, A., Majeedi, U. (2023). Role of artificial intelligence and machine learning in interventional cardiology. Current Problems in Cardiology, 48(7): 101698. https://doi.org/10.1016/j.cpcardiol.2023.101698

[12] Taye, M.M. (2023). Understanding of machine learning with deep learning: Architectures, workflow, applications and future directions. Computers, 12(5): 91.

https://doi.org/10.3390/computers12050091
[13] Galić, I., Habijan, M., Leventić, H., Romić, K. (2023). Machine learning empowering personalized medicine: A comprehensive review of medical image analysis methods. Electronics, 12(21): 4411. https://doi.org/10.3390/electronics12214411
[14] Sampath, K., Rajagopal, S., Chintanpalli, A. (2024). A comparative analysis of CNN-based deep learning architectures for early diagnosis of bone cancer using CT images. Scientific Reports, 14(1): 2144. https://doi.org/10.1038/s41598-024-52719-8
[15] Li, J., Li, S., Li, X., Miao, S., Dong, C., Gao, C., Liu, X., Hao, D., Xu, W., Huang, M., Cui, J. (2023). Primary bone tumor detection and classification in full-field bone radiographs via YOLO deep learning model. European Radiology, 33(6): 4237-4248. https://doi.org/10.1007/s00330-022-09289-y
[16] Rahman, S.M., Ibtisum, S., Bazgir, E., Barai, T. (2023). The significance of machine learning in clinical disease diagnosis: A review. arXiv Preprint arXiv: 2310.16978. https://doi.org/10.48550/arXiv.2310.16978
[17] Özyurt, F. (2021). Automatic detection of COVID-19 disease by using transfer learning of light weight deep learning model. Traitement du Signal, 38(1): 147-153. https://doi.org/10.18280/ts.380115
[18] Subasi, A., Mitra, A., Ozyurt, F., Tuncer, T. (2021). Automated COVID-19 detection from CT images using deep learning. In Computer-Aided Design and Diagnosis Methods for Biomedical Applications. CRC Press, pp. 153-176.
[19] Erdem, F., Tamsel, İ., Demirpolat, G. (2023). The use of radiomics and machine learning for the differentiation of chondrosarcoma from enchondroma. Journal of Clinical Ultrasound, 51(6): 1027-1035. https://doi.org/10.1002/jcu.23461
[20] Cilengir, A.H., Evrimler, S., Serel, T.A., Uluc, E., Tosun, O. (2023). The diagnostic value of magnetic resonance imaging-based texture analysis in differentiating enchondroma and chondrosarcoma. Skeletal Radiology, 52(5): 1039-1049. https://doi.org/10.1007/s00256-022-04242-y
[21] Anttila, T.T., Aspinen, S., Pierides, G., Haapamäki, V., Laitinen, M.K., Ryhänen, J. (2023). Enchondroma detection from hand radiographs with an interactive deep learning segmentation tool-A feasibility study. Journal of Clinical Medicine, 12(22): 7129. https://doi.org/10.3390/jcm12227129
[22] Gitto, S., Cuocolo, R., Albano, D., Chianca, V., Messina, C., Gambino, A., Ugga, L., Cortese, M.C., Lazzara, A., Ricci, D., Spairani, R., Zanchetta, E.D., Luzzati, A., Brunetti, A., Parafioriti, A., Sconfienza, L.M. (2020). MRI radiomics-based machine-learning classification of bone chondrosarcoma. European Journal of Radiology, 128: 109043. https://doi.org/10.1016/j.ejrad.2020.109043
[23] Yoon, H., Choi, W.H., Joo, M.W., Ha, S., Chung, Y.A. (2023). SPECT/CT radiomics for differentiating between enchondroma and grade i chondrosarcoma. Tomography, 9(5): 1868-1875. https://doi.org/10.3390/tomography9050148
[24] Lisson, C.S., Lisson, C.G., Flosdorf, K., Mayer-Steinacker, R., Schultheiss, M., von Baer, A., Barth, T.F.E., Beer, A.J., Baumhauer, M., Meier, R., Beer, M., Schmidt, S.A. (2018). Diagnostic value of MRI-based 3D texture analysis for tissue characterisation and discrimination of low-grade chondrosarcoma from enchondroma: A pilot study. European Radiology, 28: 468-477. https://doi.org/10.1007/s00330-017-5014-6
[25] Manganelli Conforti, P., D'Acunto, M., Russo, P. (2022). Deep learning for chondrogenic tumor classification through wavelet transform of Raman spectra. Sensors, 22(19): 7492. https://doi.org/10.3390/s22197492
[26] Gitto, S., Annovazzi, A., Nulle, K., Interlenghi, M., Salvatore, C., Anelli, V., Baldi, J., Messina, C., Albano, D., Luca, F.D., Armiraglio, E., Parafioriti, A., Luzzati, A., Biagini, R., Castiglioni, I., Sconfienza, L.M. (2024). X-Rays radiomics-based machine learning classification of atypical cartilaginous tumour and high-grade chondrosarcoma of long bones. EBioMedicine, 101. https://doi.org/10.1016/j.ebiom.2024.105018
[27] von Schacky, C.E., Wilhelm, N.J., Schäfer, V.S., Leonhardt, Y., Jung, M., Jungmann, P.M., Russe, M.F., Foreman, S.C., Gassert, F.G., Gassert, F.T., Schwaiger, B.J., Mogler, C., Knebel, C., von Eisenhart-Rothe, R., Makowski, M.R., Woertler, K., Burgkart, R., Gersing, A.S. (2022). Development and evaluation of machine learning models based on X-ray radiomics for the classification and differentiation of malignant and benign bone tumors. European Radiology, 32(9): 6247-6257. https://doi.org/10.1007/s00330-022-08764-w
[28] He, K., Zhang, X., Ren, S., Sun, J. (2016). Deep residual learning for image recognition. In Proceedings of the IEEE Conference on Computer Vision and Pattern Recognition, pp. 770-778.
[29] Dosovitskiy, A., Beyer, L., Kolesnikov, A., Weissenborn, D., Zhai, X., Unterthiner, T., Dehghani, M., Minderer, M., Heigold, G., Gelly, S., Uszkoreit, J., Houlsby, N. (2020). An image is worth 16×16 words: Transformers for image recognition at scale. https://doi.org/10.48550/arXiv.2010.11929
[30] Huang, G., Liu, Z., Van Der Maaten, L., Weinberger, K.Q. (2017) Densely connected convolutional networks. In Proceedings of the IEEE Conference on Computer Vision and Pattern Recognition, Honolulu, 4700-4708. https://doi.org/10.1109/CVPR.2017.243
[31] Goodfellow, I., Bengio, Y., Courville, A. (2016). Deep Learning. MIT Press.
[32] Shao, Z., Zhao, R., Yuan, S., Ding, M., Wang, Y. (2022). Tracing the evolution of AI in the past decade and forecasting the emerging trends. Expert Systems with Applications, 209: 118221. https://doi.org/10.1016/j.eswa.2022.118221
[33] Koch, B.J., Peterson, D. (2024). From protoscience to epistemic monoculture: How benchmarking set the stage for the deep learning revolution. arXiv Preprint arXiv: 2404.06647. https://doi.org/10.48550/arXiv.2404.06647
[34] Dong, G., Liu, H. (Eds.). (2018). Feature engineering for machine learning and data analytics. CRC Press.
[35] Zheng, A., Casari, A. (2018). Feature Engineering for Machine Learning: Principles and Techniques for Data Scientists. O'Reilly Media, Inc.
[36] Dargan, S., Kumar, M., Ayyagari, M.R., Kumar, G. (2020). A survey of deep learning and its applications: A new paradigm to machine learning. Archives of Computational Methods in Engineering, 27: 1071-1092. https://doi.org/10.1007/s11831-019-09344-w
[37] Luo, G. (2016). A review of automatic selection methods for machine learning algorithms and hyper-parameter

values. Network Modeling Analysis in Health Informatics and Bioinformatics, 5: 1-16. https://doi.org/10.1007/s13721-016-0125-6

[38] Zhou, G., Zhang, J., Su, J., Shen, D., Tan, C. (2004). Recognizing names in biomedical texts: A machine learning approach. Bioinformatics, 20(7): 1178-1190. https://doi.org/10.1093/bioinformatics/bth060

[39] Mouloodi, S., Rahmanpanah, H., Burvill, C., Martin, C., Gohari, S., Davies, H.M. (2022). How artificial intelligence and machine learning is assisting us to extract meaning from data on bone mechanics? Biomedical Visualisation. Springer, Cham, 11: 195-221. https://doi.org/10.1007/978-3-030-87779-8_9

[40] Massalimova, A., Timmermans, M., Esfandiari, H., Carrillo, F., Laux, C.J., Farshad, M., Denis, K., Fuernstahl, P. (2022). Intraoperative tissue classification methods in orthopedic and neurological surgeries: A systematic review. Frontiers in Surgery, 9: 952539. https://doi.org/10.3389/fsurg.2022.952539

[41] Hong, L., Lin, J., Li, S., Wan, F., Yang, H., Jiang, T., Zhao D, Zeng, J. (2020). A novel machine learning framework for automated biomedical relation extraction from large-scale literature repositories. Nature Machine Intelligence, 2(6): 347-355. https://doi.org/10.1038/s42256-020-0189-y

[42] LeCun, Y., Bengio, Y., Hinton, G. (2015). Deep learning. Nature, 521(7553): 436-444. https://doi.org/10.1038/nature14539

[43] Tolstikhin, I.O., Houlsby, N., Kolesnikov, A., Beyer, L., Zhai, X., Unterthiner, T., Yung, J., Steiner, A., Keysers, D., Uszkoreit, J., Lucic, M., Dosovitskiy, A. (2021). Mlp-mixer: An all-MLP architecture for vision. Advances in Neural Information Processing Systems, 34: 24261-24272.

[44] Tuncer, T., Dogan, S., Baygin, M., Tasci, I., Mungen, B., Tasci, B., Barua, P.D., Acharya, U. (2024). TTPat and CWINCA-Based explainable feature engineering model using Directed Lobish: A new EEG artifact classification model. Knowledge-Based Systems, 112555.

[45] Tuncer, T., Dogan, S., Tasci, I., Baygin, M., Barua, P.D., Acharya, U.R. (2024). Lobish: Symbolic language for interpreting electroencephalogram signals in language detection using channel-based transformation and pattern. Diagnostics, 14(17): 1987. https://doi.org/10.3390/diagnostics14171987

[46] Tuncer, T., Dogan, S., Özyurt, F., Belhaouari, S.B., Bensmail, H. (2020). Novel multi center and threshold ternary pattern based method for disease detection method using voice. IEEE Access, 8: 84532-84540. https://doi.org/10.1109/ACCESS.2020.2992641

[47] Goldberger, J., Hinton, G.E., Roweis, S., Salakhutdinov, R.R. (2004). Neighbourhood components analysis. Advances in Neural Information Processing Systems, 17: 513-520.

[48] Maillo, J., Ramírez, S., Triguero, I., Herrera, F. (2017). kNN-IS: An iterative spark-based design of the k-nearest neighbors classifier for big data. Knowledge-Based Systems, 117: 3-15. https://doi.org/10.1016/j.knosys.2016.06.012

[49] Dogan, A., Akay, M., Barua, P.D., Baygin, M., Dogan, S., Tuncer, T., Dogru A.H., Acharya, U.R. (2021). PrimePatNet87: Prime pattern and tunable q-factor wavelet transform techniques for automated accurate EEG emotion recognition. Computers in Biology and Medicine, 138: 104867. https://doi.org/10.1016/j.compbiomed.2021.104867

[50] Jabber, B., Shankar, M., Rao, P.V., Krishna, A., Basha, C.Z. (2020). SVM model based computerized bone cancer detection. In 2020 4th International Conference on Electronics, Communication and Aerospace Technology (ICECA), Coimbatore, India, pp. 407-411. https://doi.org/10.1109/ICECA49313.2020.9297624

[51] Anand, D., Arulselvi, G., Balaji, G., Chandra, G.R. (2022). A deep convolutional extreme machine learning classification method to detect bone cancer from histopathological images. International Journal of Intelligent Systems and Applications in Engineering, 10(4): 39-47.

[52] Acevedo, A., Alférez, S., Merino, A., Puigví, L., Rodellar, J. (2019). Recognition of peripheral blood cell images using convolutional neural networks. Computer Methods and Programs in Biomedicine, 180: 105020. https://doi.org/10.1016/j.cmpb.2019.105020